

Distinct effect of Kondo physics on crystal field splitting in electron and spin spectroscopies

M. Kornjača^{1,2} and R. Flint^{1,2}

¹Ames Laboratory, U.S. Department of Energy, Ames, Iowa 50011

²Department of Physics and Astronomy, Iowa State University, Ames, IA, 50011

(Dated: July 16, 2024)

Magnetic anisotropy is a key feature of rare earth materials from permanent magnets to heavy fermions. We explore the complex interplay of Kondo physics and anisotropy in a minimal impurity model using numerical renormalization group. While anisotropy suppresses Kondo physics, Kondo physics enhances the anisotropy. Importantly, we find distinct renormalization of the magnetic anisotropy measured via dynamical spin response (inelastic neutron scattering) versus electronic excitations in the impurity spectral function (resonant inelastic x-rays and scanning tunneling spectroscopy). The two measurement types have different responses and dependences on the temperature and Kondo scales.

Magnetic anisotropy in rare earth intermetallics can be exceptionally strong and useful, particularly for high performance ferromagnets[1], where it allows high coercivities. It is also an important tuning parameter for topological materials [2], and heavy fermion magnetism, superconductivity [3], and quantum criticality [4, 5]. Modeling and measuring this anisotropy is an important, but challenging problem. While the effect of anisotropy on Kondo physics has been explored [6–8], the effect of Kondo physics on the anisotropy, particularly spectroscopically, is still an open question relevant for materials with mixed valent Ce or Yb, where Kondo screening strongly renormalizes the bare f levels.

Localized rare earth f electrons have large Coulomb interactions (\sim eV) and spin-orbit couplings (\sim 100 meV) that lead to well defined total J multiplets that could undergo $SU(N = 2J+1)$ Kondo screening, or be split by the much weaker crystalline electronic field (CEF) (\sim meV) into doublets with highly anisotropic moments. The CEF splitting protects this magnetic anisotropy, and can be measured by fitting thermodynamic data or by inelastic neutron scattering (INS) [9], as well as photoemission [10–16], resonant inelastic x-ray scattering (RIXS) [17–23], time-domain THz spectroscopy [24, 25] and scanning tunneling microscopy (STM) [26–28]. Even without Kondo, computing the CEF splitting in intermetallics is difficult [29, 30], making accurate measurements even more important. Kondo broadening of the spectral peaks [31] makes measurements difficult, particularly for mixed valent materials, and it can sometimes be hard to reconcile CEF measurements from different techniques [17].

The effect of CEF splitting, Δ on impurity Kondo physics has been theoretically examined with exact results [32, 33], poor man’s scaling [6], the non-crossing approximation [7, 34–38] and the numerical renormalization group (NRG) [8]. The simplest $SU(4)$ case captures the main physics: without CEF splitting, there is a large, $SU(4)$ Kondo temperature, T_K at which the entire quartet is screened, but this fixed point is marginally unstable to any Δ , which suppresses the Kondo screening until

the excited doublet is totally unoccupied and the ground state doublet is screened at an exponentially suppressed $SU(2)$ Kondo temperature. This crossover from $SU(4)$ to $SU(2)$ Kondo occurs as a function of Δ/T_K , and can be seen in many thermodynamic quantities [8, 33, 39].

In this paper, we explore the effect of valence fluctuations on magnetic anisotropy using NRG [8, 40, 41] studies of an anisotropic $SU(4)$ Anderson model with a CEF split $J = 3/2$ quartet, where we find two distinct spectroscopic signatures of the CEF splitting. The first is a splitting of the Kondo resonance in the impurity spectral function, $A(\omega)$ that corresponds to a renormalized CEF splitting (Δ^*) between low-lying, magnetic “broken Kondo singlet” states, which are observable by effectively electronic probes like photoemission, RIXS and STM. The second is the peak in the INS response, $S(\omega)$ corresponding to excitations between the ground state and excited state Kondo singlets at low temperatures (ω_\perp). The two features are related, but clearly distinct, as they are affected differently by temperature, the degree of valence fluctuations and the ratio of Δ/T_K . The renormalized CEF scale, Δ^* is generically enhanced by the development of valence fluctuations at intermediate temperatures, while the INS peak, ω_\perp is more weakly, but monotonically enhanced with increasing temperature. Interestingly, this enhancement mostly happens well above T_K where the moments remain largely un-screened, suggesting that Kondo physics could enhance the anisotropy near the operating temperatures of high performance permanent magnets.

We consider the magnetic anisotropy in a minimal, $J = 3/2$ Anderson impurity model with a tetragonal CEF splitting the quartet into two doublets, $|\Gamma_{7\pm}\rangle = |J_z = \pm 3/2\rangle$ and $|\Gamma_{6\pm}\rangle = |J_z = \pm 1/2\rangle$. To keep the model generic, we denote the ground state doublet as $|f_{1\sigma}^\dagger\rangle$ and the excited state as $|f_{2\sigma}^\dagger\rangle$. Each doublet hybridizes through a single conduction channel, resulting in

the Hamiltonian,

$$H = \sum_{\mathbf{k}\alpha\sigma} \epsilon(\mathbf{k}) c_{\mathbf{k}\alpha\sigma}^\dagger c_{\mathbf{k}\alpha\sigma} + \epsilon_f n_{f1} + (\epsilon_f + \Delta) n_{f2} + U \sum_{\alpha\sigma \neq \alpha'\sigma'} n_{f\alpha\sigma} n_{f\alpha'\sigma'} + \sum_{\mathbf{k}\sigma\alpha} [V_\alpha(\mathbf{k}) c_{\mathbf{k}\alpha\sigma}^\dagger f_{\alpha\sigma} + h.c.]. \quad (1)$$

$f_{\alpha\sigma}^\dagger$ creates an impurity site fermion in doublet $\alpha = 1, 2$ with spin $\sigma = \pm$; $n_{f\alpha\sigma} = f_{\alpha\sigma}^\dagger f_{\alpha\sigma}$ and $n_{f\alpha} = \sum_{\sigma} n_{f\alpha\sigma}$. $c_{\mathbf{k}\alpha\sigma}^\dagger$ creates a conduction electron that hybridizes with doublet α , via the hybridization V_α . $\epsilon_f < 0$ is the impurity chemical potential, and Δ is the bare CEF splitting. We include a simple impurity interaction, U for clarity, but take U to be effectively infinite, prohibiting any double occupancy and making our model an infinite- U Anderson model. The relevant energy levels and parameters are sketched in the inset of Fig. 1. The impurity physics is completely described by the local impurity Hamiltonian and corresponding hybridization functions [41]:

$$\Gamma_\alpha(\omega) = \pi \sum_{\mathbf{k}} \delta(\omega - \epsilon(\mathbf{k})) |V_\alpha(\mathbf{k})|^2. \quad (2)$$

In the remainder of the paper, we consider a flat conduction electron density of states and isotropic, $V_1 = V_2 = V$ hybridization functions constant within $[-D, D]$, where D is the conduction electron bandwidth.

We solve this model using NRG [40–43], employing the NRG Ljubljana open source package [44, 45]. In NRG, the Anderson impurity model is mapped to a finite chain with a logarithmic discretization of the continuous conduction bath, with discretization parameter $\Lambda > 1$. The exact limit corresponds to $\Lambda \rightarrow 1$, but larger Λ can allow for more efficient calculations if the resulting finite size effects are minimized by averaging over N_z discretization realizations; we use the Campo-Olivera scheme as implemented by NRG Ljubljana [44, 46]. The diagonalization of the chain Hamiltonian is performed iteratively, with a basis truncation at each iteration that keeps maximum m states. NRG Ljubljana enforces the relevant symmetries, which lowers the required m ; as we do not consider external fields, we use the full $SU(2)$ spin symmetries for each doublet, and the overall $U(1)$ charge symmetry. Unless otherwise indicated, we set $\Lambda = 4$, $N_z = 4$ and $m = 1500$, which allows for good convergence of both thermodynamic quantities and spectroscopic functions. We also fix $U = 100$, $D = 1$, $V = 0.113$, with $\Gamma_0 = \frac{1}{2D}\pi V^2 = 0.02$, and vary $|\epsilon_f|$ and Δ . Our results are consistent with previous work on the same model [8], where applicable. Other checks and error estimates are discussed in the Supplementary Material (SM) [47].

To examine the spectroscopic signatures of the magnetic anisotropy in this model, we calculate the frequency dependent impurity spectral functions (Fig. 1) and dynamical spin susceptibilities (Fig. 2), and examine how the different peaks evolved with temperature, Δ and ϵ_f .

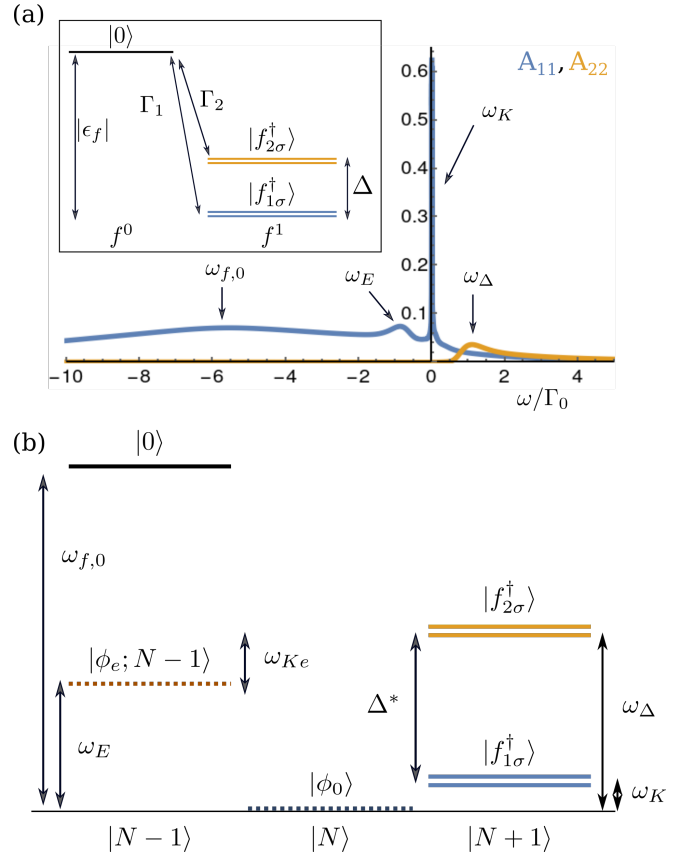


FIG. 1. (a) Example NRG impurity spectral function, with the ground state (A_{11}) and excited state (A_{22}) spectral functions in blue and orange, for $|\epsilon_f|/\Gamma_0 = 8$, $\Delta/\Gamma_0 = 1$, $T/\Gamma_0 = 0.0001$. (Inset) The $J = 3/2$ infinite- U Anderson model has two f^1 doublets split by Δ , $|f_{\alpha\sigma}^\dagger\rangle = |J_z = \pm \frac{3}{2}\rangle, |J_z = \pm \frac{1}{2}\rangle$, and an excited empty state (f^0) with energy cost $|\epsilon_f|$; other atomic configurations are forbidden. The doublets hybridize, $\Gamma_{1,2}$ through two conduction channels, allowing for perfect screening. (b) The four spectral function peaks capture charged excitations ($N \rightarrow N \pm 1$) out of the ground state Kondo singlet, $|\phi_0\rangle$ [7]. The sharp central peak, ω_K corresponds to the Kondo resonance for breaking the Kondo singlet by adding an f_1 ; $\omega_\Delta = \omega_K + \Delta^*$ corresponds to adding an f_2 ; $\omega_{f,0} = |\epsilon_f^*|$ is the empty state; and $\omega_E = \Delta^* - \omega_{EK}$ corresponds to removing an f_1 into an energy range overlapping the excited Kondo singlet, $|\phi_e; N-1\rangle$, with energy lowered from the uncorrelated excited doublet by ω_{Ke} ; $N-1$ indicates the lower conduction electron count.

We calculate the impurity spectral function for both ground and excited state electrons, f_1 and f_2 . It is instructive to consider the $T = 0$ spectral function,

$$A_{\alpha\alpha}(\omega) = \sum_{\sigma} \sum_N |\langle N | f_{\alpha\sigma}^\dagger | \phi_0 \rangle|^2 \delta(\omega + E_0 - E_N). \quad (3)$$

The sum is over many-body states $|N\rangle$, and $\alpha = 1, 2$ labels the ground and excited CEF states. At $T = 0$, $A_{\alpha\alpha}(\omega)$ measures the probability to add or remove elec-

trons from the ground state Kondo singlet:

$$|\phi_0\rangle = \left[u + \sum_{\mathbf{k}\alpha\sigma} v_{\mathbf{k}\alpha} f_{\alpha\sigma}^\dagger c_{\mathbf{k}\alpha\sigma} \right] |\text{FS}; f^0\rangle, \quad (4)$$

where $|\text{FS}\rangle$ is the N electron Fermi sea. While at $T = 0$, $|\phi_0\rangle$ is the only occupied Kondo singlet, for large enough Δ there is an unoccupied excited state Kondo singlet,

$$|\phi_e\rangle = \left[u_e + \sum_{\mathbf{k}\alpha\sigma} v_{e,\mathbf{k}\alpha} f_{\alpha\sigma}^\dagger c_{\mathbf{k}\alpha\sigma} \right] |\text{FS}; f^0\rangle. \quad (5)$$

There are up to four distinct peaks in the spectral functions [7], as seen in Fig. 1: two ways to add an electron (f_1 : ω_K or f_2 : ω_Δ) to the ground state Kondo singlet ($\omega > 0$), thereby breaking it, and two ways to remove an electron ($\omega < 0$): either into the empty state, $|f^0\rangle$: $\omega_{f,0}$ or the empty part of the excited Kondo singlet: ω_E . The temperature dependence of the peaks is shown in Fig. 3.

The renormalized CEF splitting shows up here as a splitting of the two $\omega > 0$ peaks that add either f_1 or f_2 electrons to $|\phi_0\rangle$. For $\Delta = 0$, there is just one Kondo resonance, essentially corresponding to the energy cost for breaking the ground state Kondo singlet, which is only possible because of the admixture of the empty state into the Kondo singlet, u , as double occupancy is prohibited. Finite Δ splits it into two peaks, similarly to magnetic field for $SU(2)$ Kondo physics [48–50], and the weight of each peak is $2n_0$, where n_0 is the occupancy of the empty state. We label the two peaks ω_K and ω_Δ .

The asymmetric lower Kondo resonance is phenomenologically fit by a generalized Fano-Frota form [50, 51],

$$A_{GF}(\omega) = A_0 \text{Re} \left\{ e^{i\phi} \left[\frac{i\Gamma}{\omega - \omega_0 + i\Gamma} \right]^a \right\}. \quad (6)$$

The Frota form, $\frac{2}{\pi\Gamma_0} \text{Re} \left[\sqrt{\frac{i\Gamma}{\omega - \omega_0 + i\Gamma}} \right]$ has long been used to model Kondo resonance peaks in the symmetric $SU(2)$ Anderson model, with the square-root motivated by orthogonality catastrophe physics [52, 53]. We generalize the power law $a = 1 - 2(\delta/\pi)^2$, $\delta = \pi/N$ from $N = 2$, which gives the usual $SU(2)$ $a = 1/2$, to interpolate between $SU(2)$ and $SU(4)$ with a more general power law $1/2 < a < 7/8$. ϕ allows a Fano asymmetry, which was introduced to fit STM Kondo resonances, where the asymmetry comes from co-tunneling [50, 51]; here the asymmetry is intrinsic to the infinite- U Anderson model [54]. To compensate for some low frequency numerical artifacts (see discussion in SM [47]), we fit this peak with $A_{GF}(\omega)$ and define ω_K , Γ_K to be the peak location and half-width-half-maximum of the fitted curve. $\omega_K(T)$ initially increases with T and then decreases again as the peak broadens, persisting to $\sim 10T_K$.

The CEF peak is located at $\omega_\Delta \geq \omega_K$, with $\Gamma_\Delta > \Gamma_K$, where Γ_Δ is generically renormalized by the interactions to be much narrower than the non-interacting width, Γ_0 .

We interpret the splitting, $\Delta^* = \omega_\Delta - \omega_K$ as the renormalized CEF scale, which is enhanced by up to 40% from the bare Δ , as seen in Fig. 4. For $\Delta \lesssim \omega_K$, the peak is well-fit by the generalized Fano-Frota form, but not for larger Δ , where it is no longer a Kondo resonance [47]. $\omega_\Delta(T)$ also increases with T , and the peak broadens and persists well above $T \sim \Delta, T_K$.

Now we turn to $\omega < 0$. Both f_1 and f_2 electrons can be removed from the Kondo singlet into the empty, f^0 state, which has two peaks. The first is the usual broad f^0 peak, whose energy is renormalized to $\omega = -\omega_{f_0} = \epsilon_f^*$. The second peak is the excited Kondo resonance, at $\omega = -\omega_E = -(\Delta^* - \omega_{K_e})$, which corresponds to excitations into the f^0 (u_e) part of the unoccupied excited Kondo singlet ($|\phi_e\rangle$), where there is a pileup of f^0 weight at ω_{K_e} below the renormalized Δ^* [7]. This peak is often discussed as a CEF “side-band” with $\omega_E = \omega_\Delta$ mirrored from $\omega > 0$ [15, 16, 24, 37]; however, while this is roughly true for large Δ , we generically find ω_E to be substantially smaller than ω_Δ , due to $\omega_{K_e} \gg \omega_K$; the two peaks also have opposite T dependences, with this peak tending to narrow slightly and move towards $\omega = 0$ with increasing temperature.

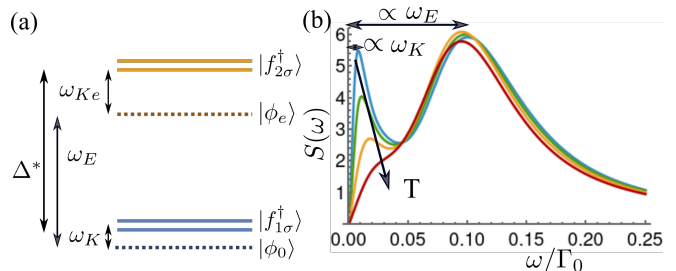


FIG. 2. (a) Relevant energy levels for neutral magnetic excitations out of the ground state Kondo singlet, $|\phi_0\rangle$. The low-lying magnetic excitations to the broken Kondo singlet states, $|f_{\alpha\sigma}^\dagger\rangle$ manifest as peaks in $\chi''_{\alpha\alpha}(\omega)$, while $\chi''_{\perp}(\omega)$ appears to be dominated by excitations between the ground and excited Kondo singlets. (b) Temperature dependence of the INS structure factor, $S(\omega)$ for $\Delta/\Gamma_0 = 0.1$, $\epsilon_f/\Gamma_0 = -8$. Temperatures are $0.003\Gamma_0$ (blue), $0.006\Gamma_0$ (green), $0.01\Gamma_0$ (orange), $0.02\Gamma_0$ (red), which are all at or above the Kondo temperature, $T_K \sim 0.003\Gamma_0$, defined as the temperature below which the empty state occupancy, $n_0(T)$ saturates. The lower peak is associated with the Kondo resonance ($\propto \omega_K$), and shifts and broadens significantly with T , while the upper CEF peak ($\propto \omega_E$) shifts slightly without much broadening.

While the spectral function tells us about charge excitations, the dynamical spin susceptibilities tell us about the neutral magnetic excitations. There are three relevant susceptibilities that contribute to the INS signal shown in Fig. 2: intra-doublet susceptibilities, $\chi_{\alpha\alpha}(\omega) = \int dt e^{i\omega t} \langle S_{z,\alpha}(t) S_{z,\alpha}(0) \rangle$, where $S_{z,\alpha} = \sum_{\sigma} \sigma f_{\alpha\sigma}^\dagger f_{\alpha\sigma}$, and the inter-doublet susceptibility,

$$\chi_{\perp}(\omega) = \int dt \langle J_x(t) J_x(0) \rangle e^{-i\omega t}, \quad (7)$$

where $J_x = \sum_{\sigma} f_{1\sigma}^{\dagger} f_{2\sigma} + f_{2\sigma}^{\dagger} f_{1\sigma}$ allows transitions between the two doublets. In the absence of magnetic field, $\chi_{\alpha\alpha}$ are $SU(2)$ symmetric; these were also looked at previously [8]; χ_{12} is uniformly zero (as is A_{12}). However, all three components, including the previously uncalculated χ_{\perp} are necessary to calculate the INS structure factor:

$$S(\omega) \propto n_B(\omega) \left\{ \frac{1}{3} \left[\left(\frac{3}{2} \right)^2 \chi''_{11}(\omega) + \left(\frac{1}{2} \right)^2 \chi''_{22}(\omega) \right] + \frac{2}{3} \left[\chi''_{22}(\omega) + \left(\frac{\sqrt{3}}{2} \right)^2 \chi''_{\perp}(\omega) \right] \right\}. \quad (8)$$

$S(\omega)$ is the powder-averaged neutron structure factor for the $J = 3/2$ doublet in tetragonal symmetry, where the first, second terms are the J_z, J_x response, respectively and $n_B(\omega)$ is the Bose factor [47]. Here, we choose the ground and excited state doublets to be $|\pm 3/2\rangle$ and $|\pm 1/2\rangle$, respectively, giving an Ising anisotropy. To understand the different magnetic excitations in Fig. 2(a), we look at the three component susceptibilities, with the temperature dependence of the peaks reported in Fig. 3.

At low temperatures, $\chi''_{\alpha\alpha}(\omega)$ are inelastic, with peaks at $\omega_{11} \approx 1.3\omega_K$, $\omega_{22} \approx 1.3\omega_{\Delta}$, where the proportionality factor for these peaks is consistently between 1.2 – 1.4 at the lowest temperatures. These responses arise from magnetic excitations between the ground state Kondo singlet and low energy excited states with f_{α} character, which are essentially broken Kondo singlet states. These magnetic excitations occur at slightly enhanced frequencies compared to the charge excitations measured by $A_{\alpha\alpha}(\omega)$, but are the same fundamental physics[7]. As T increases, there is a crossover from inelastic to quasi-elastic behavior, diagnosed by the absence of peaks in $\chi''(\omega)/\omega$ [47, 55]. χ''_{11} becomes quasi-elastic around T_K , while χ''_{22} becomes quasi-elastic between T_K and Δ .

The inter-doublet susceptibility, $\chi''_{\perp}(\omega)$ captures fluctuations out of the ground state Kondo singlet into an excited state with f_2 character, ω_{\perp} or, if there is f_2 weight in the ground state, into an excited state with f_1 character, at ω_{11} . The f_2 excited state could either be the excited Kondo resonance, at $\approx \omega_E$, or an unscreened f_2 state, at $\approx \omega_{\Delta}$. We only ever observe one peak, at $\omega_{\perp} < \omega_{22}$, aside from the peak at ω_{11} for sufficiently small Δ . ω_{22} and ω_{11} share the temperature dependence of ω_K and ω_{Δ} , respectively, with a constant of proportionality ~ 1.3 . ω_{\perp} has much more in common with ω_E , but with a more variable proportionality factor ranging from 1 – 2 with changing Δ and ϵ_f , with larger values for larger Δ/ω_K . Both ω_{\perp} and ω_E decrease with increasing temperature, increase with increasing Δ and remain basically flat with increasing $|\epsilon_f|$. Both peaks survive without significant broadening to much higher temperatures than $\omega_{\alpha\alpha}$. As such, we identify the main peak, ω_{\perp} in $S(\omega)$ at low temperatures with excitations from the ground state to the excited state Kondo singlet, $\omega_E = \Delta^* - \omega_{K_e}$, dis-

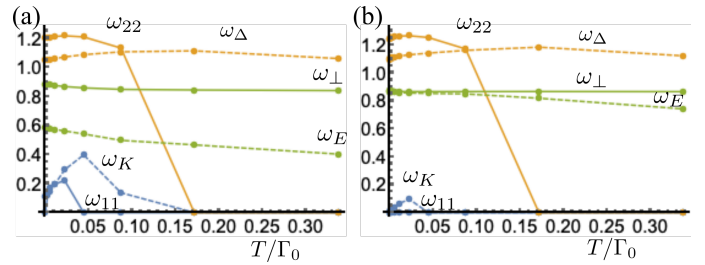


FIG. 3. Temperature dependent peak locations from $A(\omega)$ [ω_K , ω_{Δ} and ω_E] and $\chi''(\omega)/\omega$ [ω_{11} , ω_{22} and ω_{\perp}], for (a) $\Delta/\Gamma_0 = 1$, $\epsilon_f/\Gamma_0 = -6$, (b) $\Delta/\Gamma_0 = 1$, $\epsilon_f/\Gamma_0 = -8$. The peaks in $\chi''(\omega)/\omega$ (for $\chi = \chi_{\alpha\alpha}$ and χ_{\perp}) are only non-zero for inelastic behavior, with the quasi-elastic peaks at zero; when the behavior is inelastic, the electronic spectral and spin susceptibility peaks are roughly proportional; the Kondo resonance peaks, ω_K and ω_{11} (in blue) are both multiplied by a factor of 20. Notably, the monotonic decrease with temperature of ω_{\perp} and ω_E (in green) is similar, and distinct from the other two peaks, which are more dome-like. However, the relationship between the overall scale, ω_{\perp}/ω_E varies significantly with ϵ_f , likely due to increasing mixed valency.

tinct from the Δ^* measured by electron spectroscopies.

In general, the INS structure factor has two peaks: ω_{11} and ω_{\perp} with very different temperature dependences, as seen in Fig. 2(b). While the lower Kondo resonance could be mistaken for an “extra” CEF peak in a single temperature scan [56], it moves and broadens substantially with temperature, while the CEF peak at ω_{\perp} is relatively temperature independent.

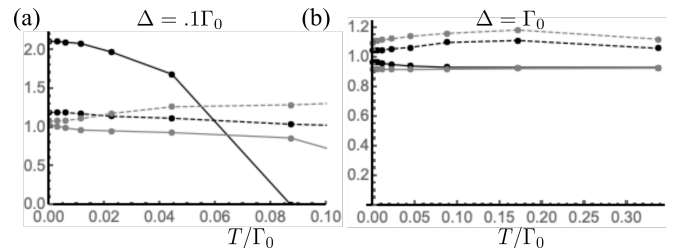


FIG. 4. Temperature dependence of the two measures of effective CEF splitting: $\Delta^*(T)$ (dashed lines) and ω_{\perp} (solid lines), both in units of the bare Δ . Different colors indicate different $\epsilon_f/\Gamma_0 = -6$ (black), -8 (gray). (a) shows the behavior for $\Delta/\Gamma_0 = 0.1$, where the Kondo scales are roughly $\omega_K/\Gamma_0 = 0.08, 0.002$. The temperature scale is cut off at $T = \Delta$, where the peaks become very broad and χ_{\perp} becomes quasi-elastic. $\epsilon_f/\Gamma_0 = -6$ exemplifies the behavior for $\Delta \lesssim \omega_K$, where ω_{\perp} is substantially enhanced by valence fluctuations, particularly compared to Δ^* . (b) shows the temperature dependence for $\Delta/\Gamma_0 = 1$, where the Kondo scales are roughly $\omega_K/\Gamma_0 = 0.005, 0.0001$. Higher Kondo temperatures lead to larger enhancement in ω_{\perp} at low temperatures, agreeing with poor man’s scaling, while lower Kondo temperatures lead to more enhancement in Δ^* for the same Δ .

In conclusion, our NRG results show quite distinct behavior in the electronic response, or impurity spectral

function effectively measured by photoemission, RIXS and STM, compared to the dynamical spin response measured by INS. This difference is enhanced by valence fluctuations that substantially renormalize both measures, as seen in Fig. 4. This work sheds light on how different measurements of the CEF scale are connected to the underlying theoretical models, and when different techniques really are measuring different physical quantities, as for $\Delta \lesssim T_K$ [17], or the same quantity, for $\Delta \gg T_K$.

We can understand the behavior of the two Kondo resonance peaks in $A(\omega)$, where both peaks increase and broaden initially with as the temperature increases past T_K , as the Kondo singlet melts and low-lying magnetic states are thermally populated, smearing out the $f^0 - f^1_\alpha$ transition signature. The effective CEF splitting, $\Delta^*(T) = \omega_\Delta - \omega_K$ represents the difference in how the split peaks smear, which is a good proxy for how the low-lying magnetic states are split. This splitting of the low-lying magnetic states also manifests in the difference of the χ''_{11} and χ''_{22} dynamical spin responses, whose difference is proportional to Δ^* . Interestingly, most variation in Δ^* occurs *well* above T_K , typically where the valence, $n_f(T)$ is also changing significantly.

By contrast, the CEF scale measured by INS, ω_\perp uniformly increases with decreasing temperature, with changes occurring closer to T_K . We interpret ω_\perp as the energy difference between the ground and excited state Kondo singlets, which is more directly measured by the $\omega_E = \Delta^* - \omega_{Ke}$ peak seen in $A_{11}(\omega < 0)$. Interestingly, this response follows what is expected from anisotropic $SU(4)$ poor man's scaling [57]. For the relatively symmetric case considered here, $\Gamma_\alpha = \Gamma_0$, there are two relevant Kondo scales, $J_\pm = \frac{1}{2}(J_1 \pm J_2)$, where J_α are associated with the ground and excited state doublets, $J_\alpha(T = \infty) = \Gamma_\alpha$. $J_\pm > 0$ both flow to strong coupling, with $J_+ = J_-$ at the anisotropic $SU(2)$ fixed point. The CEF splitting is initially enhanced by valence fluctuations as $\partial\Delta/\partial \log D \propto -\rho J_+ J_-$, consistent with the behavior of $\omega_\perp \sim \omega_E$, but not really that of Δ^* . Previous NRG and poor man's scaling work on the larger S anisotropic $SU(2)$ Kondo model with single-ion anisotropy has found anisotropy switching even for initially isotropic ($J_z = J_\perp$) Kondo [58], unlike here, indicating a key difference between the spin- S $SU(2)$ Kondo relevant for generic transition metals [49, 58–61] and the anisotropic $SU(N)$ Kondo relevant for rare earths. Our $\Gamma_\alpha = \Gamma_0$ results likely represent minimal changes in Δ^* , ω_\perp , as the enhancement can be much larger for $\Gamma_2 < \Gamma_1$, and for $\Gamma_2 > \Gamma_1$, J_- can be negative and drive CEF inversions [58, 62–64]; how this inversion manifests in the different spectroscopic and thermodynamic responses is an interesting question for future work.

We acknowledge stimulating discussions with Joseph Eix, Filip Ronning, Benjamin Ueland. This work was supported by the U.S. Department of Energy, Office of Science, Basic Energy Sciences, Materials Science and

Engineering.

-
- [1] R. McCallum, L. Lewis, R. Skomski, M. Kramer, and I. Anderson, *Annual Review of Materials Research* **44**, 451 (2014), <https://doi.org/10.1146/annurev-matsci-070813-113457>.
 - [2] Y. Lee, R. Skomski, X. Wang, P. P. Orth, Y. Ren, B. Kang, A. K. Pathak, A. Kutepov, B. N. Harmon, R. J. McQueeney, I. I. Mazin, and L. Ke, *Phys. Rev. B* **108**, 045132 (2023).
 - [3] P. Pagliuso, N. Curro, N. Moreno, M. Hundley, J. Thompson, J. Sarrao, and Z. Fisk, *Physica B: Condensed Matter* **320**, 370 (2002), proceedings of the Fifth Latin American Workshop on Magnetism, Magnetic Materials and their Applications.
 - [4] Q. Y. Chen, D. F. Xu, X. H. Niu, J. Jiang, R. Peng, H. C. Xu, C. H. P. Wen, Z. F. Ding, K. Huang, L. Shu, Y. J. Zhang, H. Lee, V. N. Strocov, M. Shi, F. Bisti, T. Schmitt, Y. B. Huang, P. Dudin, X. C. Lai, S. Kirchner, H. Q. Yuan, and D. L. Feng, *Phys. Rev. B* **96**, 045107 (2017).
 - [5] S. Kirchner, S. Paschen, Q. Chen, S. Wirth, D. Feng, J. D. Thompson, and Q. Si, *Rev. Mod. Phys.* **92**, 011002 (2020).
 - [6] K. Hanzawa, K. Yamada, and K. Yosida, *Journal of Magnetism and Magnetic Materials* **47-48**, 357 (1985).
 - [7] N. E. Bickers, D. L. Cox, and J. W. Wilkins, *Phys. Rev. B* **36**, 2036 (1987).
 - [8] F. B. Anders and T. Pruschke, *Phys. Rev. Lett.* **96**, 086404 (2006).
 - [9] T. Willers, Z. Hu, N. Hollmann, P. O. Körner, J. Gegner, T. Burnus, H. Fujiwara, A. Tanaka, D. Schmitz, H. H. Hsieh, H.-J. Lin, C. T. Chen, E. D. Bauer, J. L. Sarrao, E. Goremychkin, M. Koza, L. H. Tjeng, and A. Severing, *Phys. Rev. B* **81**, 195114 (2010).
 - [10] J. W. Allen, *Journal of the Physical Society of Japan* **74**, 34 (2005), <https://doi.org/10.1143/JPSJ.74.34>.
 - [11] Y.-X. Duan, C. Zhang, J. Ruzs, P. M. Oppeneer, T. Durakiewicz, Y. Sassa, O. Tjernberg, M. Månsson, M. H. Berntsen, F.-Y. Wu, Y.-Z. Zhao, J.-J. Song, Q.-Y. Wu, Y. Luo, E. D. Bauer, J. D. Thompson, and J.-Q. Meng, *Phys. Rev. B* **100**, 085141 (2019).
 - [12] Q. Y. Chen, C. H. P. Wen, Q. Yao, K. Huang, Z. F. Ding, L. Shu, X. H. Niu, Y. Zhang, X. C. Lai, Y. B. Huang, G. B. Zhang, S. Kirchner, and D. L. Feng, *Phys. Rev. B* **97**, 075149 (2018).
 - [13] S. Patil, A. Generalov, M. Güttler, P. Kushwaha, A. Chikina, K. Kummer, T. C. Rödel, A. F. Santander-Syro, N. Caroca-Canales, C. Geibel, S. Danzenbächer, Y. Kucherenko, C. Laubschat, J. W. Allen, and D. V. Vyalikh, *Nature Communications* **7**, 11029 (2016).
 - [14] D. V. Vyalikh, S. Danzenbächer, Y. Kucherenko, K. Kummer, C. Krellner, C. Geibel, M. G. Holder, T. K. Kim, C. Laubschat, M. Shi, L. Patthey, R. Follath, and S. L. Molodtsov, *Phys. Rev. Lett.* **105**, 237601 (2010).
 - [15] F. Reinert, D. Ehm, S. Schmidt, G. Nicolay, S. Hüfner, J. Kroha, O. Trovarelli, and C. Geibel, *Phys. Rev. Lett.* **87**, 106401 (2001).
 - [16] D. Ehm, S. Hüfner, F. Reinert, J. Kroha, P. Wölffe, O. Stockert, C. Geibel, and H. v. Löhneysen, *Phys. Rev.*

- B **76**, 045117 (2007).
- [17] A. Amorese, G. Dellea, M. Fanciulli, S. Seiro, C. Geibel, C. Krellner, I. P. Makarova, L. Braicovich, G. Ghiringhelli, D. V. Vyalikh, N. B. Brookes, and K. Kummer, *Phys. Rev. B* **93**, 165134 (2016).
- [18] A. Amorese, N. Caroca-Canales, S. Seiro, C. Krellner, G. Ghiringhelli, N. B. Brookes, D. V. Vyalikh, C. Geibel, and K. Kummer, *Phys. Rev. B* **97**, 245130 (2018).
- [19] A. Amorese, K. Kummer, N. B. Brookes, O. Stockert, D. T. Adroja, A. M. Strydom, A. Sidorenko, H. Winkler, D. A. Zocco, A. Prokofiev, S. Paschen, M. W. Haverkort, L. H. Tjeng, and A. Severing, *Phys. Rev. B* **98**, 081116 (2018).
- [20] A. Amorese, O. Stockert, K. Kummer, N. B. Brookes, D.-J. Kim, Z. Fisk, M. W. Haverkort, P. Thalmeier, L. H. Tjeng, and A. Severing, *Phys. Rev. B* **100**, 241107 (2019).
- [21] B. T. Chioigo, J. Okamoto, J.-H. Li, T. Ohkochi, H.-Y. Huang, D.-J. Huang, C.-T. Chen, C.-N. Kuo, C.-S. Lue, A. Chainani, and D. Malterre, *Phys. Rev. B* **106**, 075141 (2022).
- [22] A. Amorese, P. Hansmann, A. Marino, P. Körner, T. Willers, A. Walters, K.-J. Zhou, K. Kummer, N. B. Brookes, H.-J. Lin, C.-T. Chen, P. Lejay, M. W. Haverkort, L. H. Tjeng, and A. Severing, *Phys. Rev. B* **107**, 115164 (2023).
- [23] D. S. Christovam, M. Ferreira-Carvalho, A. Marino, M. Sundermann, D. Takegami, A. Melendez-Sans, K. D. Tsuei, Z. Hu, S. Rößler, M. Valvidares, M. W. Haverkort, Y. Liu, E. D. Bauer, L. H. Tjeng, G. Zwicknagl, and A. Severing, *Phys. Rev. Lett.* **132**, 046401 (2024).
- [24] S. Pal, C. Wetli, F. Zamani, O. Stockert, H. v. Löhneysen, M. Fiebig, and J. Kroha, *Phys. Rev. Lett.* **122**, 096401 (2019).
- [25] P. Shee, C.-J. Yang, S. Kumar Pandey, A. Kumar Nandy, R. Kulkarni, A. Thamizhavel, M. Fiebig, and S. Pal, *Phys. Rev. B* **109**, 075133 (2024).
- [26] L. Jiao, S. Rößler, D. Kim, L. H. Tjeng, Z. Fisk, F. Steglich, and S. Wirth, *Nature Communications* **7**, 13762 (2016).
- [27] S. Ernst, S. Kirchner, C. Krellner, C. Geibel, G. Zwicknagl, F. Steglich, and S. Wirth, *Nature* **474**, 362 (2011).
- [28] M. Haze, R. Peters, Y. Torii, T. Suematsu, D. Sano, M. Naritsuka, Y. Kasahara, T. Shibauchi, T. Terashima, and Y. Matsuda, *Journal of the Physical Society of Japan* **88**, 014706 (2019), <https://doi.org/10.7566/JPSJ.88.014706>.
- [29] F. Zhou and V. Ozoliņš, *Phys. Rev. B* **80**, 125127 (2009).
- [30] Y. Lee, Z. Ning, R. Flint, R. J. McQueeney, I. I. Mazin, and L. Ke, “Toward a first-principles theory of rare-earth ions in crystals,” (2024), [arXiv:2024.XXXX \[cond-mat.str-el\]](https://arxiv.org/abs/2024.XXXX).
- [31] A. D. Christianson, E. D. Bauer, J. M. Lawrence, P. S. Riseborough, N. O. Moreno, P. G. Pagliuso, J. L. Sarrao, J. D. Thompson, E. A. Goremychkin, F. R. Trouw, M. P. Hehlen, and R. J. McQueeney, *Phys. Rev. B* **70**, 134505 (2004).
- [32] P. Schlottmann, *Phys. Rev. B* **30**, 1454 (1984).
- [33] H.-U. Desgranges, *Physica B: Condensed Matter* **473**, 93 (2015).
- [34] V. Zevin, G. Zwicknagl, and P. Fulde, *Phys. Rev. Lett.* **60**, 2331 (1988).
- [35] J. E. Han, M. Alouani, and D. L. Cox, *Phys. Rev. Lett.* **78**, 939 (1997).
- [36] P. S. Riseborough, *Phys. Rev. B* **67**, 045102 (2003).
- [37] J. Kroha, S. Kirchner, G. Sellier, P. Wölfle, D. Ehm, F. Reinert, S. Hübner, and C. Geibel, *Physica E: Low-dimensional Systems and Nanostructures* **18**, 69 (2003), 23rd International Conference on Low Temperature Physics (LT23).
- [38] N. O. Moreno, A. Lobos, A. A. Aligia, E. D. Bauer, S. Bovev, V. Fritsch, J. L. Sarrao, P. G. Pagliuso, J. D. Thompson, C. D. Batista, and Z. Fisk, *Phys. Rev. B* **71**, 165107 (2005).
- [39] P. Schlottmann, *Physics Reports* **181**, 1 (1989).
- [40] K. G. Wilson, *Rev. Mod. Phys.* **47**, 773 (1975).
- [41] R. Bulla, T. A. Costi, and T. Pruschke, *Rev. Mod. Phys.* **80**, 395 (2008).
- [42] H. R. Krishna-murthy, J. W. Wilkins, and K. G. Wilson, *Phys. Rev. B* **21**, 1003 (1980).
- [43] W. Hofstetter, *Phys. Rev. Lett.* **85**, 1508 (2000).
- [44] R. Žitko and T. Pruschke, *Phys. Rev. B* **79**, 085106 (2009).
- [45] R. Žitko, “Nrg ljubljana,” (2021).
- [46] V. L. Campo and L. N. Oliveira, *Phys. Rev. B* **72**, 104432 (2005).
- [47] See Supplementary Material below.
- [48] A. Rosch, T. A. Costi, J. Paaske, and P. Wölfle, *Phys. Rev. B* **68**, 014430 (2003).
- [49] R. Žitko, R. Peters, and T. Pruschke, *New Journal of Physics* **11**, 053003 (2009).
- [50] R. Žitko, *Phys. Rev. B* **84**, 195116 (2011).
- [51] H. Prüser, M. Wenderoth, A. Weismann, and R. G. Ulbrich, *Phys. Rev. Lett.* **108**, 166604 (2012).
- [52] H. O. Frota, *Phys. Rev. B* **45**, 1096 (1992).
- [53] S. Doniach and M. Sunjic, *Journal of Physics C: Solid State Physics* **3**, 285 (1970).
- [54] A. K. Zhuravlev, V. Y. Irkhin, M. I. Katsnelson, and A. I. Lichtenstein, *Phys. Rev. Lett.* **93**, 236403 (2004).
- [55] S. Hoshino, J. Otsuki, and Y. Kuramoto, *Journal of the Physical Society of Japan* **78**, 074719 (2009), <https://doi.org/10.1143/JPSJ.78.074719>.
- [56] R. A. Robinson, M. Kohgi, T. Osakabe, F. Trouw, J. W. Lynn, P. C. Canfield, J. D. Thompson, Z. Fisk, and W. P. Beyermann, *Phys. Rev. Lett.* **75**, 1194 (1995).
- [57] J. Eix and R. Flint, “Anisotropic kondo scaling in a $j = 3/2$ kondo impurity with crystal field (in preparation),” (2024).
- [58] M. P. Kwasigroch, H. Hu, F. Krüger, and A. G. Green, *Phys. Rev. B* **105**, 224418 (2022).
- [59] R. Žitko, R. Peters, and T. Pruschke, *Phys. Rev. B* **78**, 224404 (2008).
- [60] A. F. Otte, M. Ternes, K. von Bergmann, S. Loth, H. Brune, C. P. Lutz, C. F. Hirjibehedin, and A. J. Heinrich, *Nature Physics* **4**, 847 (2008).
- [61] M. Höck and J. Schnack, *Phys. Rev. B* **87**, 184408 (2013).
- [62] K. Hattori, *Journal of the Physical Society of Japan* **79**, 114717 (2010), <https://doi.org/10.1143/JPSJ.79.114717>.
- [63] L. V. Pourovskii, P. Hansmann, M. Ferrero, and A. Georges, *Phys. Rev. Lett.* **112**, 106407 (2014).
- [64] J.-P. Rueff, J. M. Ablett, F. Strigari, M. Deppe, M. W. Haverkort, L. H. Tjeng, and A. Severing, *Phys. Rev. B* **91**, 201108 (2015).

Supplemental Material: “Distinct effects of Kondo physics on crystal field splitting in electronic and spin spectroscopies”

In this supplemental material, we discuss how well our NRG results satisfy the expected sum rules in Section I; discuss the estimated numerical error in the spectral function peak locations in section II; provide several example spectral functions and structure factors to show the temperature evolution of Δ^* and ω_\perp discussed in the main paper in section III; provide examples of the evolution of dynamical susceptibilities from inelastic to quasi-elastic as a function of temperature in section IV; and finally provide additional details of the derivation of the inelastic neutron scattering response in section V.

SUM RULE CHECKS

We can do several checks, beyond convergence, to make sure our numerical results are well-behaved. In a finite- U model, we expect $\sum_i \int_{-\infty}^{\infty} A_{\alpha\alpha}(\omega) d\omega = 4$. In our case, we set $U = 100$, which is much much larger than all of the other energy scales in the problem, and so double occupancy is effectively eliminated. The integral of $A_{\alpha\alpha}(\omega)$ up to the Fermi energy ($\omega = 0$) gives the particle density in orbital α ,

$$n_\alpha(T) = 2 \int_{-\infty}^0 A_{\alpha\alpha}(\omega, T) d\omega \quad (9)$$

so we can obtain n_1 and n_2 , with $n_0 = 1 - n_1 - n_2$ being the occupancy of the excited empty state. The positive frequencies then correspond to all the ways that electrons can be added to this system, which are limited because of the infinite U . Basically, $n_0 f_{\alpha\sigma}$ electrons can be added to get up to total $n = 1$. However, because there are $N = 4$ ways to add electrons, the total weight of $\sum_\alpha \int_0^\infty A_{\alpha\alpha}(\omega) d\omega = 4n_0$. This sum rule is satisfied with an error of $\approx .1\%$ for all cases considered here, and is unaffected by decreasing Λ or increasing the number of kept states, m .

We also expect the Friedel sum rule to be satisfied at zero temperature, which is a relationship between $A_{\alpha\alpha}(0)$ for a single spin component and the phase shifts,

$$A_{\alpha\alpha}(0) = \frac{1}{\pi\Gamma_0} \sin^2\left(\frac{\pi n_\alpha}{2}\right). \quad (10)$$

Here, we use the $A_{\alpha\alpha}(0)$ of the fitted functions for the lowest temperatures calculated ($T_0 = .0001\Gamma_0$), and find that the Friedel sum rule is satisfied within $\approx 0.4 - 5\%$. These are not improved by increasing m or decreasing the Λ , and the largest “errors” are for smaller T_K systems and likely arise almost entirely from the finite temperature.

Finally, we can check the $\Delta = 0$ results with the n_0 for the Bethe ansatz $J = 3/2$ calculation [39]. For example, with $\epsilon_f = -6\Gamma_0$, at the lowest temperature, $T = 0.0001\Gamma_0$, we find $n_f = n_1 + n_2 = .826$, while the Bethe Ansatz predicts $n_f = .824$ at $T = 0$, which agrees to $< .2\%$, with some discrepancy expected due to the small finite temperature.

ERROR ESTIMATES

Most of the computations in this paper were run with cutoff $\Lambda = 4$, $m = 1500$ kept states and $N_z = 4$ discretization realizations. At these values, the f -sum rule and Friedel sum rule are well satisfied, but there can be considerable numerical artifacts in the low temperature, low frequency behavior. In order to check convergence of the peak locations and to make a very crude error estimate, we ran a series of calculations for $\epsilon_f = -8\Gamma_0$, $\Delta = 0.1\Gamma_0, 1.0\Gamma_0$ and $T = 0.0001\Gamma_0$ and $0.17\Gamma_0$. In these, we chose $\Lambda = 2.5, 3.5, 4$, $m = 1500$ or 2000 , and $N_z = 4, 8$ discretization realizations. Increasing N_z from 4 to 8 made no observable differences.

For $\Delta = 0.1\Gamma_0$, the results are shown in Fig. 5, and there was no systematic change in either peak location at either temperature. We fit the peak locations for each data set, where the Kondo resonance peaks are fit with generalized Fano-Frota functions, and then the maximum of that function is taken as the peak location, in order to avoid the effects of low frequency numerical artifacts. The crystal field (CEF) peak is always just the frequency that maximizes $A_{22}(\omega)$. We estimate that the low temperature peaks are at $\omega_K/\Gamma_0 = 0.0030 \pm 0.0001$ and $\omega_\Delta/\Gamma_0 = 0.110 \pm 0.001$, giving $\Delta^*/\Gamma_0 = 0.107 \pm .001$. We estimate that the higher temperature peaks are at $\omega_K/\Gamma_0 = 0.0325 \pm 0.008$, and $\omega_\Delta/\Gamma_0 = 0.163 \pm 0.009$, giving $\Delta^*/\Gamma_0 = 0.13 \pm 0.01$.

For $\Delta = 1.0\Gamma_0$, the results are shown in Fig. 6. Here, there is no systematic change in the Kondo resonance peaks, but the ω_Δ peak location does systematically increase with decreasing Λ for these m , suggesting that the number of

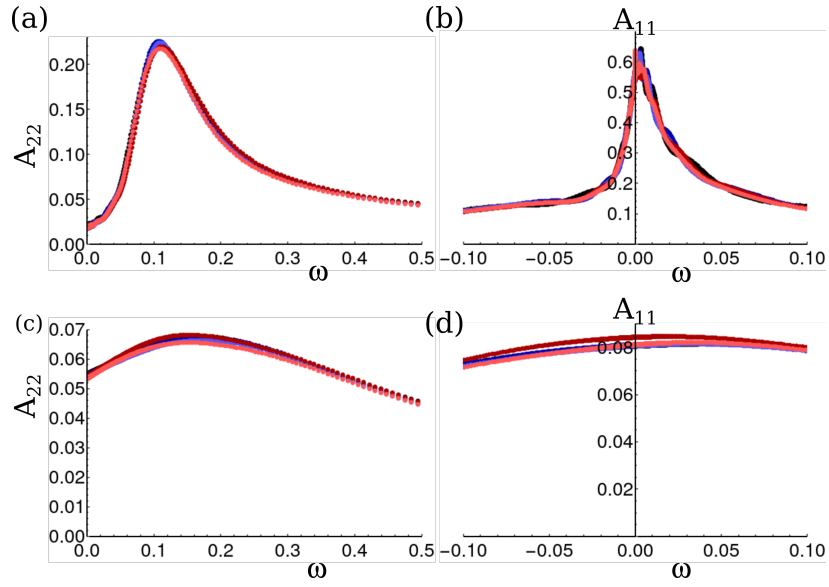


FIG. 5. Error estimates for $\Delta = .1\Gamma_0$, $\epsilon_f = -8\Gamma_0$. Five spectral function curves vs ω (in units of Γ_0) are shown in each sub-figure, calculated for $\Lambda = 4$, $m = 1500$, as in the main text (black); $\Lambda = 3.5$, $m = 1500$ (dark blue); $\Lambda = 3.5$, $m = 2000$ (light blue); $\Lambda = 2.5$, $m = 1500$ (dark red); $\Lambda = 2.5$, $m = 2000$ (light red). The top row is $T = .0001\Gamma_0$: (a) shows the peak in A_{22} , with average peak location and standard deviation: $\omega_\Delta = .110 \pm .001$; (b) shows the Kondo resonance peak in A_{11} , with $\omega_K = .0030 \pm .0001$. The bottom row shows $T = .17\Gamma_0$. (a) is the peak in A_{22} , with $\omega_\Delta = .163 \pm .009$; (b) is the Kondo resonance peak in A_{11} , with $\omega_K = .0325 \pm .008$.

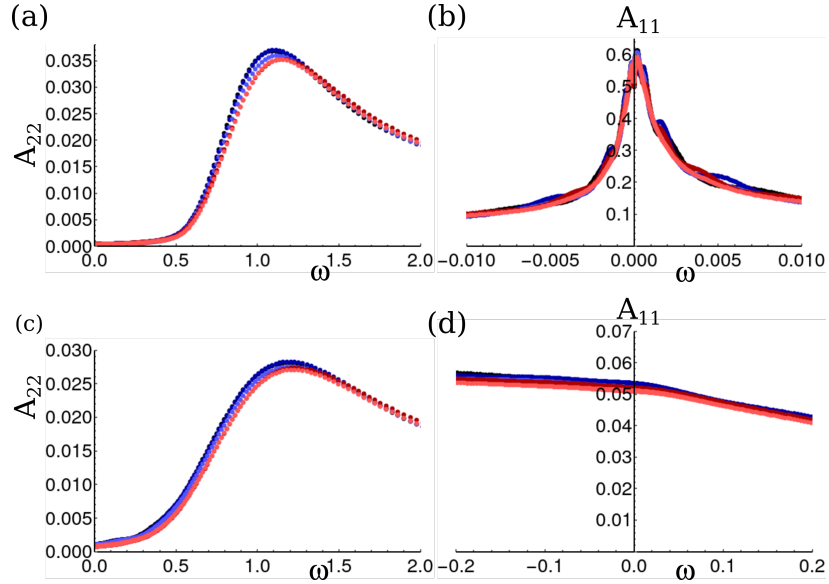


FIG. 6. Error estimates for $\Delta = 1.0\Gamma_0$, $\epsilon_f = -8\Gamma_0$. Five spectral function curves vs ω (in units of Γ_0) are shown in each sub-figure, calculated for $\Lambda = 4$, $m = 1500$, as in the main text (black); $\Lambda = 3.5$, $m = 1500$ (dark blue); $\Lambda = 3.5$, $m = 2000$ (light blue); $\Lambda = 2.5$, $m = 1500$ (dark red); $\Lambda = 2.5$, $m = 2000$ (light red). The top row is $T = .0001\Gamma_0$: (a) shows the peak in A_{22} , with an average peak location and standard deviation: $\omega_\Delta = 1.13 \pm .02$; (b) shows the Kondo resonance peak in A_{11} , with $\omega_K = .00023 \pm .00002$. The bottom row shows $T = .17\Gamma_0$. (a) is the peak in A_{22} , with $\omega_\Delta = 1.21 \pm .02$; (b) is the Kondo resonance “peak” in A_{11} , which is always at negative frequencies, and likely conflated with the excited Kondo resonance. The effective CEF splitting is just ω_Δ : $\Delta^*(.17\Gamma_0) = 1.21 \pm .02$.

kept states is insufficient for smaller Λ values. We did not find any significant change in the peak location as m was increased from 1500 to 2000, but did find that $m = 3000$ for $T = .0001\Gamma_0$, $\Lambda = 2.5$ moved the peak back to where it was for $\Lambda = 3.5$ with $m = 2000$. The quantitative error estimate for ω_Δ should be taken with a grain of salt,

but qualitatively the errors are still quite small. We fit the peak locations for each data set and did error analysis. We estimate that the low temperature peaks are at $\omega_K/\Gamma_0 = 0.00023 \pm 0.0002$ and $\omega_\Delta/\Gamma_0 = 1.13 \pm 0.02$, giving $\Delta^*/\Gamma_0 = 1.13 \pm .02$. At higher temperature, there is no Kondo resonance, and we find $\omega_\Delta/\Gamma_0 = 1.21 \pm 0.02$, giving $\Delta^*/\Gamma_0 = 1.21 \pm 0.02$ to be the enhanced CEF splitting, Δ^* .

We did not examine errors in the dynamical spin susceptibility peak locations as systematically, but they appear to be similar.

TEMPERATURE EVOLUTION OF THE SPECTRAL FUNCTION AND STRUCTURE FACTOR

In Fig. 7, we show the temperature evolution of the neutron scattering structure factor and impurity spectral functions for four cases: (a-b) $\Delta = \Gamma_0$, $\epsilon_f = -8\Gamma_0$; (c-d) $\Delta = .1\Gamma_0$, $\epsilon_f = -8\Gamma_0$; (e-f) $\Delta = \Gamma_0$, $\epsilon_f = -6\Gamma_0$; and (g-h) $\Delta = .1\Gamma_0$, $\epsilon_f = -6\Gamma_0$. The solid curves are the lowest temperature, $T_0 = .0001\Gamma_0$, which is always below the Kondo temperature; the dashed curves are $T_8 = .02\Gamma_0$, which is above the Kondo temperature except for (g-h); and the dot-dashed curves are for $T_{11} = .17\Gamma_0$, which is above all Kondo temperature scales and the bare Δ for cases (c-d) and (g-h).

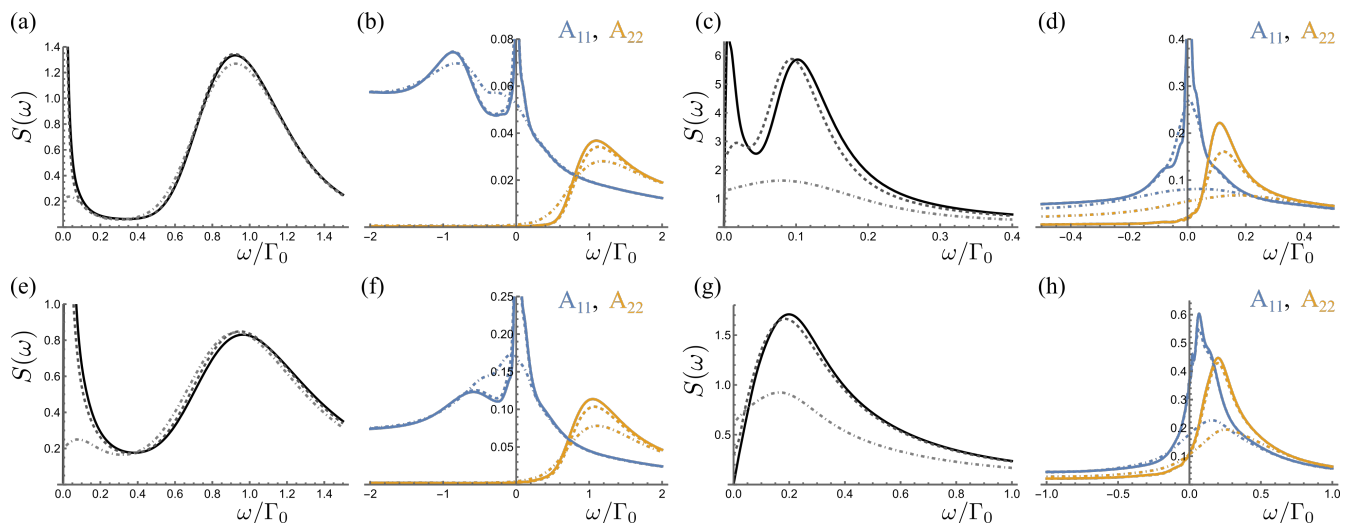


FIG. 7. Temperature dependence of the spectral functions and structure factor for: (a-b) $\Delta = \Gamma_0$, $\epsilon_f = -8\Gamma_0$; (c-d) $\Delta = .1\Gamma_0$, $\epsilon_f = -8\Gamma_0$; (e-f) $\Delta = \Gamma_0$, $\epsilon_f = -6\Gamma_0$; and (g-h) $\Delta = .1\Gamma_0$, $\epsilon_f = -6\Gamma_0$. For each pair, the left figure shows the structure factor, $S(\omega)$ used to calculate ω_\perp at three different temperatures $T_0 = .0001\Gamma_0$ (black, solid); $T_8 = .02\Gamma_0$ (dark gray, dashed); and $T_{11} = .17\Gamma_0$ (gray, dot-dashed), while the right figure shows the impurity spectral functions, $A_{\alpha\alpha}(\omega)$ used to calculate Δ^* at the same three temperatures (T_0 - solid, T_8 - dashed, T_{11} - dot-dashed). Compare to Figure 4 in the main text.

Except for (g-h), these examples all have $\Delta > \omega_K$ and exhibit $SU(2)$ Kondo physics, as can be seen from the distinction between the lower frequency Kondo resonance peaks and higher frequency CEF peaks seen in $S(\omega)$ at low temperatures. For (g-h), there is only one broad peak in $S(\omega)$ with a peak at approximately 2Δ , while in $A(\omega)$, there is a clear splitting of the Kondo resonance by the CEF, with $\Delta^* \sim 1.2\Delta$.

The change in the shape of the peak in $A_{22}(\omega)$ between more $SU(2)$ and more $SU(4)$ physics is clear here. In Fig. 8, we show the generalized Fano-Frota fits of $A_{22}(\omega)$ for case (a-b) and case (g-h), at T_0 . For case (a-b), the fit is poor and the data shows a clear gap at low frequencies, indicating this case does not behave like a Kondo resonance peak. For case (g-h), the fit is quite good, indicating that this peak should be thought of as a crystal-field split Kondo resonance. The generalized Fano-Frota fits are always good for the lower energy Kondo resonance.

INELASTIC VERSUS QUASI-ELASTIC RESPONSE

In order to understand the differences between the dynamical susceptibilities, it is useful to look at $\chi''(\omega)/\omega$, which will show a peak at finite frequencies for an inelastic response, but will have a peak at $\omega = 0$ for a Lorentzian quasi-elastic response. As can be seen in Fig. 9, the three different susceptibilities all lose their inelastic nature at different

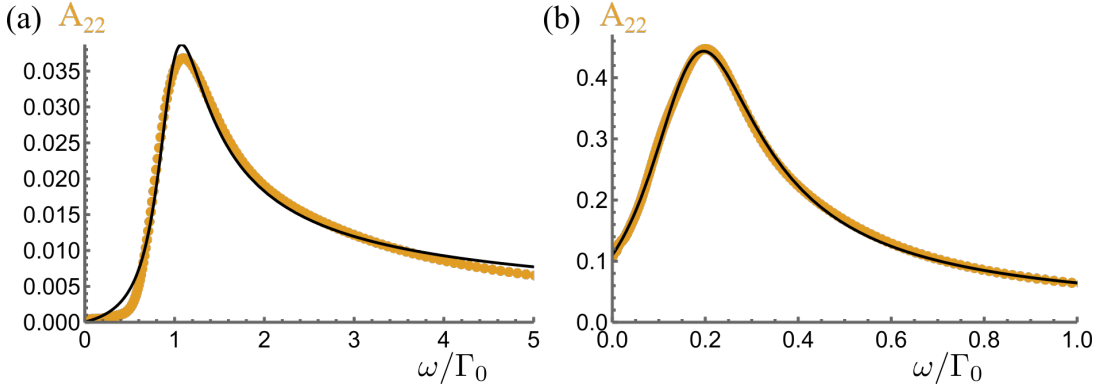


FIG. 8. Generalized Fano-Frota fits, $A_{GF}(\omega) = A_0 \text{Re} \left\{ e^{i\phi} \left[\frac{i\Gamma}{\omega - \omega_0 + i\Gamma} \right]^a \right\}$ for (a) $\Delta = \Gamma_0$, $\epsilon_f = -8\Gamma_0$ at $T_0 = .0001\Gamma_0$, where the fit is poor: fit parameters are: $A_0 = .046$, $\omega_0 = .96$, $\Gamma = .25$, $a = .64$, $\phi = .74$, all in units of Γ_0 . (b) $\Delta = 0.1\Gamma_0$, $\epsilon_f = -6\Gamma_0$ at $T_0 = .0001\Gamma_0$: fit parameters are: $A_0 = .46$, $\omega_0 = .16$, $\Gamma = .13$, $a = .88$, $\phi = -.43$. The large distinction in weights between the two peaks is due to the very small value of $n_2 = .014$ ($n_1 = .92$) at low temperatures for case (a), versus $n_2 = .28$ ($n_1 = .55$) for case (b).

temperatures, with χ_{11} becoming quasi-elastic at $\sim 10T_K$, χ_{22} becoming quasi-elastic somewhere between T_K and Δ and χ_{\perp} becoming quasi-elastic around Δ .

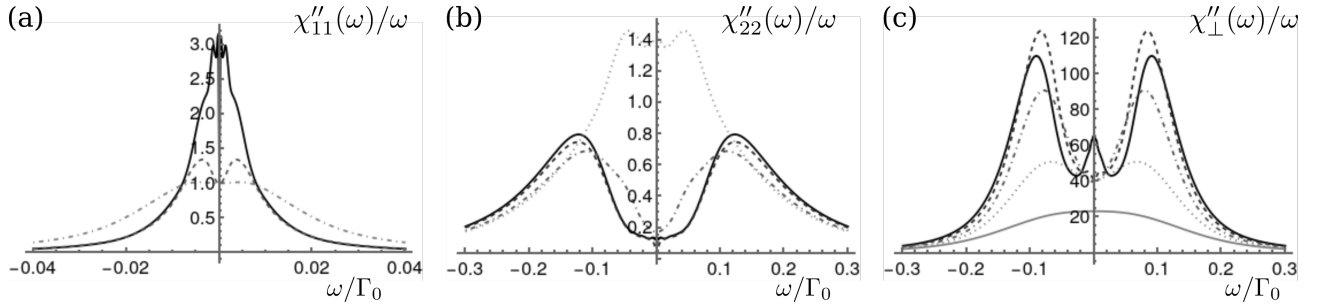


FIG. 9. The distinct temperature dependences of the three dynamical spin susceptibilities, $\chi''(\omega)/\omega$, for $\Delta = 0.1\Gamma_0$ and $\epsilon_f = -8\Gamma_0$. (a) $\chi''_{11}(\omega)/\omega$ normalized by its value at $\omega = 0$ shows how the signal for the Kondo resonance goes from inelastic to quasi-elastic as the temperature is raised from T_0 (solid, black) to T_5 (dark gray, dashed) to T_7 (gray, dot-dashed). (b) $\chi''_{22}(\omega)/\omega$ is dominated by the excited CEF scale, ω_{Δ} , and this behavior becomes quasi-elastic at a slightly higher temperature, well below Δ , with the four curves shown at T_0 (solid, black), T_5 (dark gray, dashed), T_7 (dark gray, dot-dashed), T_8 (gray, dotted). (c) $\chi''_{\perp}(\omega)/\omega$ has contributions from both the Kondo resonance and transition between the two Kondo resonances, ω_{\perp} . This peak remains quasi-elastic to much higher temperatures (roughly to $T = \Delta$) with the five curves shown at T_0 (solid, black), T_7 (dark gray, dashed), T_9 (dark gray, dot-dashed), T_{10} (gray, dotted), T_{11} (gray). The temperatures increase on a log scale, with $T_0 = .0001\Gamma_0$, $T_5 = .003\Gamma_0$, $T_7 = .01\Gamma_0$, $T_8 = .02\Gamma_0$, $T_9 = .04\Gamma_0$, $T_{10} = .09\Gamma_0$, $T_{11} = .17\Gamma_0$. The Kondo temperature for this data set is roughly T_5 , based on the temperature where $n_0(T)$ saturates.

INELASTIC NEUTRON SCATTERING

Inelastic neutron scattering to detect CEF splittings typically measures the powder average of,

$$\begin{aligned}
 S(\omega, \mathbf{Q}) &\propto n_B(\omega) \chi''(\omega, \mathbf{Q}) \\
 &\propto g_L^2 \sum_{a,b} n_a |\langle a | \mathbf{J}_{\perp} | b \rangle|^2 \delta(E_b - E_a - \hbar\omega)
 \end{aligned} \tag{11}$$

Here, n_B is the Bose function, g_L is the Lande g-factor, n_a is the thermal occupancy of $|a\rangle$, and a, b will cover the $J_z = \pm 1/2, \pm 3/2$ CEF states. $\mathbf{J}_{\perp} = \hat{Q} \times (\mathbf{J} \times \hat{Q})$ is the perpendicular component of \mathbf{J} . The powder average in a

tetragonal sample gives,

$$\chi''(\omega) \propto \sum_{a,b} n_a \left[\frac{2}{3} |\langle a|J_x|b\rangle|^2 + \frac{1}{3} |\langle a|J_z|b\rangle|^2 \right] \delta(E_b - E_a - \hbar\omega). \quad (12)$$

We can obtain this structure factor in our calculations, for a ground state doublet $|\pm 3/2\rangle$ and excited state doublet $|\pm 1/2\rangle$ as,

$$S(\omega)n_B^{-1}(\omega) \propto \frac{1}{3} \left[\left(\frac{3}{2}\right)^2 \chi''_{S,11}(\omega) + \left(\frac{1}{2}\right)^2 \chi''_{S,22}(\omega) \right] + \frac{2}{3} \left[\chi''_{S,22}(\omega) + \left(\frac{\sqrt{3}}{2}\right)^2 \chi''_{\perp}(\omega) \right]. \quad (13)$$

Here, $\chi_{S,\alpha\alpha}(\omega)$ is the S_z spin-susceptibility and $\chi_{\perp}(\omega)$ is a cross-doublet contribution to the S_x spin-susceptibility, where $J_x = \sum_{\sigma} f_{1\sigma}^{\dagger} f_{2\sigma} + f_{2\sigma}^{\dagger} f_{1\sigma}$ is used to calculate $\chi_{\perp}(\omega) = \int dt \langle J_x(t) J_x(0) \rangle e^{-i\omega t}$. We calculate all of these quantities within NRG to obtain the impurity structure factor $S(\omega)$ at different temperatures. Note that the form of this expression only depends on the identity of the “ground” and “excited” state doublets, not their actual ordering, which may evolve with temperature.